

# Pressure induced modification of the electronic properties of stilbene by two-photon spectroscopy

Cite as: J. Chem. Phys. **158**, 034505 (2023); <https://doi.org/10.1063/5.0133610>

Submitted: 04 November 2022 • Accepted: 29 December 2022 • Accepted Manuscript Online: 29 December 2022 • Published Online: 17 January 2023

 M. Agati,  S. Fanetti and  R. Bini



View Online



Export Citation



CrossMark

## ARTICLES YOU MAY BE INTERESTED IN

To age or not to age: Anatomy of a supercooled liquid's response to a high alternating electric field

The Journal of Chemical Physics **158**, 034502 (2023); <https://doi.org/10.1063/5.0138149>

Discovery of a new polymorph of clotrimazole through melt crystallization: Understanding nucleation and growth kinetics

The Journal of Chemical Physics **158**, 034503 (2023); <https://doi.org/10.1063/5.0130600>

A comprehensive benchmark ab initio survey of the stationary points and products of the OH $\cdot$  + CH $_3$ OH system

The Journal of Chemical Physics **158**, 034301 (2023); <https://doi.org/10.1063/5.0133978>

Learn More

The Journal of Chemical Physics **Special Topics** Open for Submissions

# Pressure induced modification of the electronic properties of stilbene by two-photon spectroscopy

Cite as: J. Chem. Phys. 158, 034505 (2023); doi: 10.1063/5.0133610

Submitted: 4 November 2022 • Accepted: 29 December 2022 •

Published Online: 17 January 2023



View Online



Export Citation



CrossMark

M. Agati,<sup>1</sup>  S. Fanetti,<sup>1,2</sup>  and R. Bini<sup>1,2,3,a)</sup> 

## AFFILIATIONS

<sup>1</sup> LENS, European Laboratory for Non-linear Spectroscopy, Via N. Carrara 1, Sesto Fiorentino, I-50019 Firenze, Italy

<sup>2</sup> ICCOM-CNR, Institute of Chemistry of OrganoMetallic Compounds, National Research Council of Italy, Via Madonna del Piano 10, Sesto Fiorentino, I-50019 Firenze, Italy

<sup>3</sup> Dipartimento di Chimica "Ugo Schiff" dell'Università degli Studi di Firenze, Via della Lastruccia 3, Sesto Fiorentino, I-50019 Firenze, Italy

<sup>a)</sup> Author to whom correspondence should be addressed: [roberto.bini@unifi.it](mailto:roberto.bini@unifi.it)

## ABSTRACT

Carbon nanotubes are the most exciting carbon based nanomaterials recently discovered. Obtained by compressing aromatics around 20 GPa, they are characterized by potentially exceptional mechanical properties. The reaction mechanisms have been partly elucidated through computational studies and x-ray diffraction experiments. However, in all these studies, the electronic modifications to which the molecule is subjected with increasing pressure are neglected as also if, and to which extent, the electronic excited states are involved in the high-pressure reactivity. In fact, the pressure increase induces remarkable changes in the electronic properties of molecular crystals, which are often directly related to the reaction's onset and path. We report the pressure evolution of the two-photon induced emission spectrum of crystalline stilbene, the archetype of a class of molecules from which double-core nanotubes are obtained, with the twofold purpose of gaining insight into the reaction mechanism and monitoring if the structural changes observed in x-ray diffraction studies have a detectable counterpart in the electronic properties of the system. The freezing of the spectral diffusion observed on rising pressure is ascribed to a hampered conformational rearrangement because of the larger stiffness of the local environment. The transition to the high pressure phase where the nanotubes formation is revealed by the slope change of the pressure shift of all spectral components, while the progressive intensification with pressure of the 0-0 transition suggests a strengthening of the ethylenic bond favoring the charge delocalization on the benzene moieties, which is likely the trigger of the chemical instability.

Published under an exclusive license by AIP Publishing. <https://doi.org/10.1063/5.0133610>

## I. INTRODUCTION

Carbon nanotubes are one-dimensional fully saturated polymers produced by compressing mainly aromatics and heteroaromatics above 15 GPa. The exceptional mechanical properties predicted for these diamond-like wires stem from the combination of high tensile strength with flexibility and resilience.<sup>1,2</sup> As predicted by different groups,<sup>3-5</sup> the first evidence of the nanotubes formation was obtained a few years ago by compressing benzene.<sup>6</sup> This experiment provided, through a comparative HRTEM and XRD analysis, the clue for the nanotube identification. The number

of systems investigated and of successful syntheses rapidly grew, and nanotubes were obtained by compressing aromatics such as pyridine,<sup>7,8</sup> aniline,<sup>9</sup> thiophene,<sup>10</sup> furan,<sup>11</sup> arene-perfluoroarene co-crystals,<sup>12,13</sup> pyridazine,<sup>14</sup> and s-triazine.<sup>15</sup> The variety of attainable nanotubes has recently been enriched by using as starting materials polycrystalline samples of stilbene<sup>16</sup> and other members of the pseudo-stilbene class of molecules such as azobenzene<sup>17,18</sup> and diphenylacetylene.<sup>19</sup> These molecules offer the possibility of synthesizing double core nanotubes connected through unsaturated groups that do not participate in the polymerization process, as in the case of stilbene, azobenzene, and their mixed crystals,<sup>16-18</sup> or

as observed for diphenylacetylene, through a polyacetylenic chain giving rise to the first prototypical functional application of nanothreads: a kind of semiconductive wire protected by a diamond-like sheet.<sup>19</sup> The preservation of the linking ethylenic or azo groups joined to the possibility of preparing mixed crystals of the desired relative concentration by exploiting the isomorphism of all the pseudo-stilbenes represents an appealing issue in view of designing materials with targeted electronic properties or realizing further functionalization of the nanothreads.

The reaction paths bringing to the nanothread formation can be divided into topochemical and non-topochemical. In the first case, the reaction requires minimal atomic displacement and is demonstrated to occur when the reacting molecules are organized in stacks of parallel non- or slightly displaced aromatic rings. This molecular organization is realized when adjacent molecules along the stack present opposite quadrupole moments,<sup>20</sup> as clearly demonstrated by the nanothread formation in alternate arene-perfluoroarene co-crystals<sup>13</sup> and in *s*-triazine.<sup>15</sup> In the latter, a perfect  $\pi$ - $\pi$  stacking of parallel molecules is formed with adjacent molecules along the stacks rotated by  $60^\circ$  about the principal symmetry axis.<sup>21</sup> In contrast, the herringbone-type arrangement (edge-to-face stacking), which characterizes benzene and unsubstituted aromatics, requires anisotropic stress to make the non-topochemical path competitive with the topochemical one.<sup>22,23</sup> In between these two extremes, there are several intermediate cases in which the molecules are arranged in a slipped parallel fashion, which also characterizes benzene along the *a* and *b* axes,<sup>23</sup> and depending on the distance between ring centroids, ring planes, and slippage angle, it is possible to pass with continuity from a non-topochemical to a topochemical path. This can be achieved, for example, by introducing selected substituents on the ring that modify the  $\pi$  electron density with the effect of reducing the slippage angle, thus favoring the  $\pi$ - $\pi$  interaction.<sup>24</sup>

The reactions leading to the nanothread formation have been studied by using *in situ* x-ray diffraction and vibrational spectroscopy, thus looking at the structural and bonding (hybridization) changes, but a direct characterization of how the electronic properties change with increasing the pressure has not yet been performed. This kind of study can provide information about the prereactive charge arrangement, as achieved in the case of triazine,<sup>25</sup> or about the formation of precursor species that likely trigger the chemical transformation.<sup>26</sup> Here, we report a two-photon absorption study of stilbene up to 18 GPa, thus very close to the onset of the reaction.<sup>16</sup>

The electronic spectrum of the *t*-stilbene molecule is well characterized both experimentally and theoretically (see Refs. 27 and 28 and references therein). One- and two-photon spectra markedly differ according to the centrosymmetric nature of the molecule, which restricts one- and two-photon transitions to ungerade and gerade excited states, respectively. Three two-photon transitions, all to excited  $A_g$  states, have been characterized: a weak band at about 4.3 eV, a stronger one at 5.1 eV, and the strongest peaked at about 6.4 eV.<sup>28</sup> The symmetry restrictions also apply in the crystal phase because of the inversion symmetry preservation going from the molecule to the crystal site and to the factor group ( $C_{2h}$ ).<sup>29,30</sup> One of the main reasons for studying the lower excited states has been so far related to the comprehension of the photoinduced isomerization to the *cis* form.<sup>31–34</sup> *Cis-trans* isomerization is suppressed in the crystal phase, but the study of the electronic properties of the crystal is still of interest for its sensing capabilities, which are

potentially promising for the realization of low cost large area detectors for ionizing radiation.<sup>35,36</sup> The photoluminescence induced by one-photon excitation (260–390 nm) has been studied in polycrystalline stilbene at ambient pressure in the 5–300 K temperature range.<sup>37,38</sup> The emission spectrum changes with the lowering of the temperature showing a remarkable intensification of the high energy side (bands at 344 and 369 nm), a behavior not observed when stilbene is cooled down in a polystyrene matrix. In addition, the fluorescence bands exhibit different lifetimes, an unlikely occurrence if all the bands belong to the same vibronic structure. The proposed explanation is based on the existence of emitting clusters with slightly different geometry likely related to a partial twisting of the molecule ( $\leq 16^\circ$ ).<sup>38</sup> At high temperature, the emission is fully relaxed, but on lowering the temperature, the spectral diffusion can be frozen either because the time to diffuse is longer than the lifetime of the excitation or because the system is trapped in intermediate states with energies greater than the relaxed one.

The study of the two-photon induced fluorescence as a function of pressure is, therefore, a precious source of information about the structural changes possibly induced by pressure both in the molecule and in the crystal and how they reflect on the emission properties. From this point of view, it is important to check if the suggested energetic segregation of different structural clusters also realizes under pressure and if it may possibly lead to the formation of intermediate species, potential seeds of the chemical transformation ending up in the nanothread formation.

## II. EXPERIMENTAL

Crystalline *trans*-stilbene from Sigma-Aldrich (purity  $\geq 99\%$ ) was used without any further purification. The samples were loaded without any compression medium into a membrane diamond anvil cell (MDAC) equipped with *I*ias-type diamonds (AlmaxEasyLab). Stainless steel gaskets drilled to an initial diameter of 150  $\mu\text{m}$  and a thickness of about 50  $\mu\text{m}$  were employed to contain the powder. Two-photon fluorescence spectra were measured by using as a source an optical parametric generator (Ekspla PG401), pumped by the third harmonic of a picosecond Nd:YAG laser (Ekspla PL2143A) working at a 10 Hz repetition rate. The laser beam was focused onto the sample by an achromatic doublet with a 100 mm focal length, and the sample emission was collected backward by a parabolic aluminum mirror, filtered by a monochromator, and revealed by an Electron Tubes 9235QB photomultiplier. A precise description of the setup is reported elsewhere.<sup>26,39</sup> The excitation wavelength was 600 nm, and the energy on the sample was about 100 nJ per pulse. Fluorescence spectra were measured with a resolution of about 1 nm. We did not use a ruby gauge for measuring the pressure to avoid interferences in the fluorescence measurements. The pressure was determined by the peak frequency of the two IR doublets falling, at ambient pressure, just above 1300 and around 1600  $\text{cm}^{-1}$ .<sup>16</sup> The pressure shift of these bands was previously determined by measuring the FTIR spectrum using the ruby fluorescence method for pressure calibration.<sup>40</sup> Infrared absorption spectra were measured before and after every fluorescence measurement, also with the purpose of checking sample degradation under pulsed irradiation. FTIR spectra were measured with a Bruker-IFS 120 HR spectrometer suitably modified for high pressure experiments with

an instrumental resolution of  $1 \text{ cm}^{-1}$ .<sup>41</sup> X-ray diffraction measurements were performed with a custom made laboratory diffractometer equipped with a focused Xenocs-GeniX Mo small spot microsource with a wavelength of  $0.7107 \text{ \AA}$  and a beam diameter on the focal plane of  $150 \text{ }\mu\text{m}$ . A PI-SCX 4300 CCD was employed as a detector.

### III. RESULTS

The emission spectra of stilbene have been accurately characterized in solution, in a polystyrene matrix, and in the solid state.<sup>38</sup> In solution, stilbene molecules twist in the excited state, relaxing to the ground state via a conical intersection. Twisting is already impeded in the polystyrene matrix and in the crystal. There are relevant changes in the high energy side of the emission spectrum on cooling from room temperature below  $100 \text{ K}$ .<sup>37,38,42</sup> The two higher energy bands (at about  $344$  and  $364 \text{ nm}$ ), which are much weaker than the main peak centered at about  $380 \text{ nm}$  under ambient conditions, remarkably intensify below  $200 \text{ K}$ , with the band at  $364 \text{ nm}$  becoming the strongest one. The different lifetimes measured for the high and low frequency bands of the emission spectrum suggested that they are due to multiple emitters rather than to a vibronic structure.<sup>38</sup> This interpretation is consistent with that previously advanced in Ref. 42, which attributes part of the spectral features to emission from defect levels. The higher the temperature the easier the non-radiative decay from these levels by phonon coupling. Therefore, this process requires the phonon states to be populated, thus, reducing its efficiency on cooling favoring the radiative emission. Therefore, the emission spectrum recorded at high temperature represents the fully relaxed emission, whereas the low-temperature one can be severely affected by defect levels, originated by clusters of molecules characterized by different permanent twisting with respect to the planar configuration, where excitation is trapped during the relaxation process.<sup>38</sup>

The pressure evolution of the fluorescence spectrum of crystalline stilbene was recently reported up to  $16 \text{ GPa}$ , looking for a pressure induced enhancement of the emission.<sup>43</sup> The changes in the observed emission intensities were related to modifications of the torsion angle with a consequent alteration of the intermolecular interactions and, thus, the efficiency of non-radiative relaxation channels. Surprisingly, density functional theory (DFT) calculations indicated a continuous increase of the torsion angle with pressure above  $3 \text{ GPa}$ . Compression up to  $16 \text{ GPa}$  was performed using  $\text{CCl}_4$  as the pressure transmitting medium, and neither structural changes were deduced by x-ray diffraction measurements, contrary to what was reported in Ref. 16, nor sample damages due to excitation with the  $355 \text{ nm}$  laser line.

In this study, we have characterized the fluorescence of crystalline stilbene excited by two-photon (TP) absorption as a function of pressure up to  $18 \text{ GPa}$ . The advantages of TP absorption spectroscopy in high-pressure experiments with respect to one-photon spectroscopy are well recognized.<sup>26</sup> Hydrocarbons absorption lie around or below  $300 \text{ nm}$ , thus close to or even overlapping the diamond absorption edge, especially as the pressure increases. The signal discrimination of the micron size sample embedded in mm size diamonds is, therefore, extremely difficult and is achieved by exploiting the quadratic dependence of the TP signal on the exciting photons, which entails a very high spatial selectivity. In addition, the small cross section of TP transitions minimizes the amount of

excited molecules, thus reducing the probability of triggering photochemical reactions. We used  $600 \text{ nm}$  as the excitation wavelength, which corresponds to a TP energy of about  $4.15 \text{ eV}$ . At ambient pressure, this energy corresponds to the onset of the first TP allowed transition to the  $2^1A_g$  state, which peaked at  $4.81 \text{ eV}$  and the weakest among the lower transitions to the  $A_g$  states.<sup>28</sup> Both issues are extremely important to avoid undesired photoinduced reactions, which, however, are observed after the measurement of a few pressure points.

In Fig. 1, we report the TP induced fluorescence spectra as a function of pressure up to  $4.4 \text{ GPa}$ . The ambient pressure spectrum is also measured with the sample in the DAC without applying any pressure to the diamonds. Despite that, the spectrum is less resolved than those reported at ambient temperature in the previous studies,<sup>37,38,42</sup> where it was also possible to observe the electronic origin around  $344 \text{ nm}$ , which is instead missing in our spectrum. Contrary to that reported in Ref. 43, the spectrum suddenly changes on increasing the pressure to  $0.5 \text{ GPa}$  in a very similar way to what is observed on lowering the temperature below  $200 \text{ K}$ :<sup>37,38,42</sup> the band at about  $368 \text{ nm}$  remarkably intensifies, becoming the strongest one. This band is also the only one exhibiting a blue shift, from  $368$  to  $364 \text{ nm}$ , which instead characterizes most of the emission bands on lowering the temperature at ambient pressure.<sup>37,38,42</sup> The emission

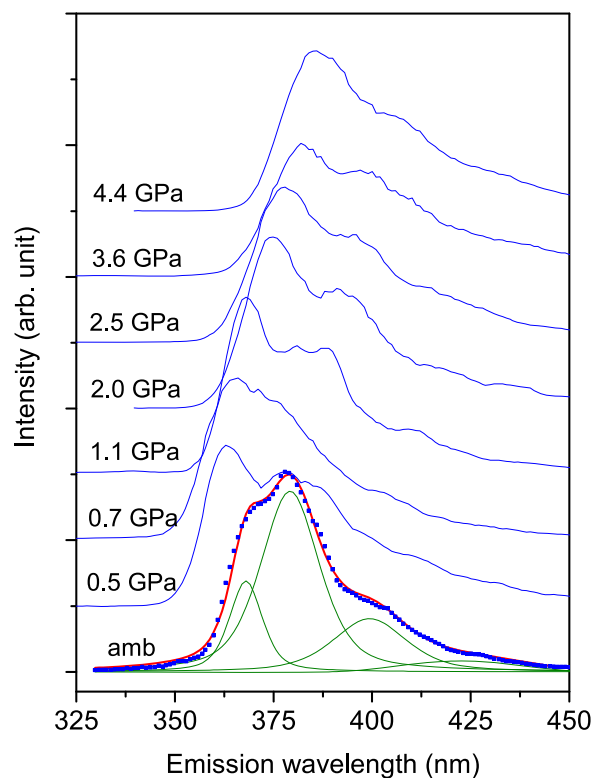


**FIG. 1.** Evolution of the emission spectrum with pressure below  $5 \text{ GPa}$ . The spectrum measured at ambient pressure has been deconvoluted, as shown in the bottom trace. The high energy band, which is at ambient pressure by far weaker than that at about  $380 \text{ nm}$ , shifts at a lower wavelength and becomes the strongest peak as the pressure is increased to  $0.5 \text{ GPa}$ .

pattern could be nicely reproduced up to 8 GPa using four bands, as shown in Fig. 1 for the spectrum measured at ambient pressure. The details of the fit procedure can be found in the [supplementary material](#). On increasing pressure up to about 8 GPa, all the bands red shift and broaden, not showing significant changes of the relative intensities. Around 8 GPa, the spectra start to change, and a new band must be considered in the fit procedure to reproduce the high energy side of the emission spectrum (see Fig. 2). This band is clearly visible only above 11 GPa (see Fig. S1) because of its intensification with increasing pressure combined with a slightly smaller red shift than all the other bands. In contrast with the continuous weakening of the other bands, the new band remarkably intensifies with pressure becoming the strongest one around 15 GPa. This behavior can be appreciated from the pressure evolution of the areas of all the bands reported in Fig. 3. The frequency separation among the different emission bands is variable, basically decreasing with rising pressure below 8 GPa and showing the opposite behavior above this pressure. The appearance of the new peak is not the only modification we detected around 8 GPa. The deconvolution of the experimental spectra also provides evidence of a clear slope change of the

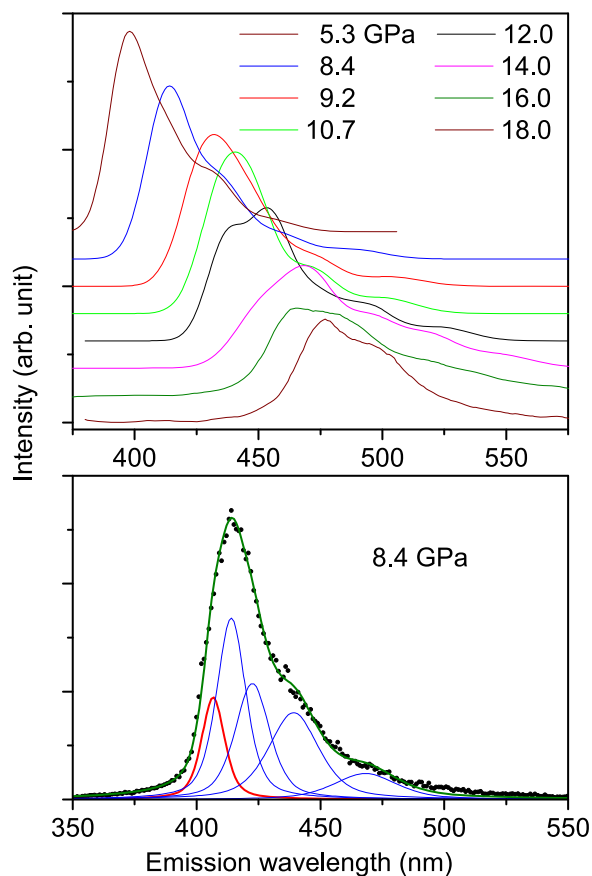


**FIG. 2.** Upper panel: evolution of the emission spectrum with pressure above 5 GPa. Lower panel: deconvolution of the 8.4 GPa emission spectrum where the new high energy band at 406 nm (red trace) appeared at about 8 GPa. This band is well visible (upper panel) as a pronounced shoulder at 12 GPa, becoming the strongest one around 15 GPa.

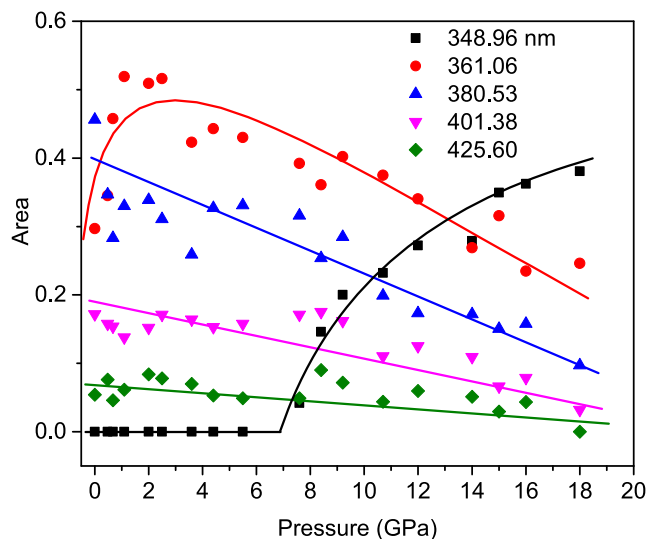


**FIG. 3.** Pressure evolution of the bands' area as obtained by the deconvolution of the experimental emission spectra. Full lines are guides for the eye. The wavelength reported in the inset are the values obtained at  $P = 0$  by the linear fit of the wavelength data, as reported in Table I.

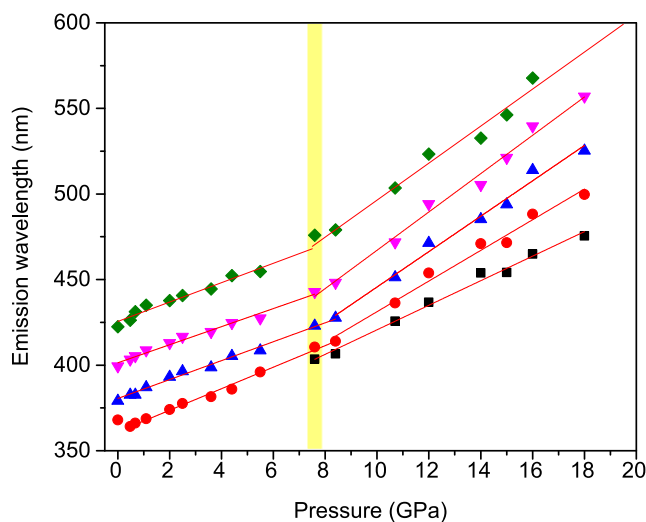


**FIG. 4.** Pressure shift of the peak maxima as obtained by the deconvolution of the experimental emission spectra. Full lines are the linear regression of the data.

pressure shift of all the different spectral components, as reported in Fig. 4. The slope increase has been quantified through the linear regression of the data below and above 8 GPa (see Table I) with the intercepts, relative to the wavelength pressure shift below and above this pressure, located between 7.2 and 8.0 GPa. Another interesting result of this analysis is the extrapolated wavelength at  $P = 0$  of the new band appearing at 8 GPa. This value, 348.96 nm, is indeed in excellent agreement with the values measured at 15 (348 nm<sup>38</sup>) and 5 K (347 nm<sup>37</sup>) for the band assigned to the 0-0 transition.



**TABLE I.** Parameters relative to the linear fit of the pressure shift of the peak as obtained by the deconvolution of the experimental emission spectra. The first column reports the literature data,<sup>38</sup> the two central columns report the slope (*a*) and the intercept (*b*) of the linear fit below and above 8 GPa, whereas in the last column are reported the pressures where the two linear fit intercept.

$\lambda_{\max}$		$\lambda = aP + b$ (0–8 GPa)		$\lambda = aP + b$ (8–18 GPa)		Intercept (GPa)
300 K	15 K	a	b	a	b	
344	348	...	...	7.17	348.96	
369	364	6.29	361.06	8.95	341.72	7.27
380	385	5.53	380.53	10.34	342.28	7.95
403	407	5.28	401.38	11.20	355.19	7.81
...	...	5.65	425.60	10.82	388.20	7.24

#### IV. DISCUSSION

There is a general consensus in explaining the ambient pressure fluorescence spectrum of crystalline stilbene and its evolution on decreasing temperature on the basis of a defect model. The strong intensification of the high energy emission bands with lowering the temperature was explained by Hochstrasser with a high concentration of defect levels that may be depopulated through coupling with lattice phonons that are significantly populated at sufficiently high temperatures. Further insight in the emission spectrum was gained by the polarization ratio, whose remarkable increase on the high frequency side indicates that this band should be ascribed to the free exciton emission.<sup>42</sup> An analogous interpretation is also given by Ostapenko *et al.* by studying the excitation spectra using different excitation wavelengths.<sup>37</sup> The dishomogeneous intensification of the emission components on lowering the temperature suggested a different origin of these bands. Excitation spectra independent on the excitation wavelength were recorded only for the two high energy bands, 348 and 367 nm, which were, therefore, assigned to the 0-0 transition and to a vibronic band. Further insight on the nature of the emission bands was given by Karpicz *et al.*,<sup>38</sup> which measured the fluorescence lifetime for all of them finding a consistent difference between the high energy band and the others, especially those at the lowest energy. This was taken as an evidence that the low energy bands have not vibronic origin and are ascribable to independent emitters, likely clusters of molecules having different configurations which, according to quantum chemical calculations, are related to a variability of the twisting angle around the C=C central bond.

All these studies agree in identifying the absorption band at 348 nm (15 K) as the origin of the  $S_1 \rightarrow S_0$  transition, while the rest of the spectrum, with maybe the exception of the 369 nm band, which has vibronic character, is related to a density distribution of localized states associated with clusters of molecules with different arrangements of the phenyl rings causing a variability in the molecular environment and, thus, a rupture of the translational symmetry.<sup>44</sup> Hopping among the different minima is thermally activated, and if the energy required to overcome the barriers separating the different local configurations is comparable to or lower than the  $kT$ , the process can be phonon assisted. Lowering the temperature implies a greater difficulty to overcome the barrier, and the excitation may decay before the system relax to a new minimum. Spectral

diffusion is, therefore, kinetically frozen, also preventing the access to lower energy defect levels, thus also explaining the blue shift of the high energy bands on lowering the temperature.<sup>45</sup> A strong support for this picture comes from the low temperature x-ray diffraction studies, where thermodynamic non-equilibrium states generated by fast freezing of conformational interconversion were observed depending on the cooling rate.<sup>29</sup>

A very similar effect to that observed when the temperature is lowered below 200 K is detected by increasing the pressure at ambient temperature: the band at 361 nm remarkably intensifies and blue shifts as the pressure is raised to 0.5 GPa, thus showing a clear resemblance with the ambient pressure behavior on cooling.<sup>37,38</sup> As mentioned before, the depopulation of higher energy lattice phonon states on lowering the temperature can reduce the spectral diffusion. An ambient temperature pressure increase does not modify the  $kT$  but shifts to higher energy the phonon density of states, thus, in principle, producing an analogous effect to lower the temperature. However, the exciton–phonon coupling is not the only mechanism that can force the emission from higher energy states. The density increase, due to the volume reduction with lowering the temperature or with increasing the pressure, can significantly alter the intermolecular interactions, possibly leading to an increase of the energy required to jump from one local configuration to another.

To this regard, a comparison of the effects of temperature and pressure on the volume of the crystal can be obtained by x-ray diffraction. Single crystal experiments have been performed at ambient<sup>30</sup> and low (113 K)<sup>46</sup> temperatures. The crystal structure of stilbene is monoclinic,  $P2_1/c$ , with two almost planar molecules in the asymmetric unit cell located at inversion centers and with one of them characterized by orientational disorder.<sup>29,30</sup> This disorder is dynamic since the occupancy of the different orientations changes with temperature.<sup>29</sup> The volume of the unit cell has been measured at different temperatures down to 90 K,<sup>29,30,46</sup> reducing from 1029.9 Å<sup>3</sup> at 295 K<sup>30</sup> to 993.7–995.9 Å<sup>3</sup> at 90 K depending on the cooling rate and, therefore, on the amount of the degree of conformational disorder.<sup>29</sup> The volume decrease in this temperature range is, therefore,  $\leq 3\%$ . The volume decrease is definitely more pronounced when the pressure is increased, as expected for molecular crystals, which are very soft materials. Single crystal data are not available at high pressure and ambient temperature powder compression experiments without a pressure transmitting medium, the

same conditions we adopted in the present study, do not provide data below 1 GPa, the pressure range where we observe the major changes in the high frequency side of the emission spectrum.<sup>16</sup> We have, therefore, recorded the XRD pattern of stilbene powder without pressure transmitting medium at 0.5 GPa measuring a volume of  $951.1 \text{ \AA}^3$ . The volume reduction from ambient conditions,  $V = 1029.9 \text{ \AA}^3$ , is about 8%, roughly three times larger than that observed on cooling. The details of the XRD measurement and data analysis can be found in the [supplementary material](#).

To check the efficiency of phonon assisted processes, we can instead rely on the lattice phonons Raman spectra measured as a function of temperature and pressure. The Raman spectrum of lattice phonons blue shifts with pressure, but still remains well below  $200 \text{ cm}^{-1}$  (KT at ambient temperature) up to 1.5 GPa,<sup>47</sup> making unlikely a decrease in the efficiency of phonon assisted processes with increasing the pressure at ambient temperature. In addition, considering the effect of temperature alone, it is difficult to ascribe the strong intensification of the high energy emission bands to phonon assisted processes since it is almost concluded at  $170 \text{ K}$ <sup>37</sup> temperature, where the KT is about  $120 \text{ cm}^{-1}$  thus including all the Raman lattice phonon bands.<sup>47</sup> The modification of the local force field due to the density increase appears, therefore, as the main reason for the localization of the emission on the vibronic band at about 360 nm. Access to lower energy defect states is prevented by the increased stiffness of the local environment, which substantially rises the energy to be overcome.

With further increasing the pressure, a slope change occurs in the pressure shift of all the emission bands at about 8 GPa. This modification is joined to the appearance of a new high energy band, which was assigned to the electronic origin because of the nice agreement of the extrapolated ambient pressure wavelength with that reported in the literature.<sup>37,38,42</sup> The new band intensifies upon compression, becoming the strongest one above 14 GPa. A phase transition around 8 GPa was already reported for stilbene, azobenzene, and the 1:1 mixed crystal in x-ray diffraction studies of powders compressed without pressure transmitting medium.<sup>16,18</sup> The transition is likely isostructural and consists of a sudden jump of about  $5^\circ$  in the monoclinic angle and a discontinuity in the volume evolution with pressure. The pressure of the transition increases to about 10 GPa when a quasi-hydrostatic pressure-transmitting is employed showing also a reversibility, which is instead not observed without a pressure transmitting medium.<sup>18</sup> In this high pressure phase, the reaction leading to the nanothreads occurs, and it was, therefore, speculated that the molecular arrangement in this phase could favor the formation of stacks where the molecules were parallel or nearly parallel arranged in order to favor the interaction along the stacks leading to the nanothread formation.

The first electronic excited state of stilbene  $S_1$ ,  $1^1B_u$  considering the  $C_{2h}$  point group notation, is characterized by the HOMO-LUMO single excitation mainly localized on the ethylenic moiety as also results from the lengthening of the corresponding C=C bond.<sup>48</sup> Despite that, the isolated molecule is considered planar also in this excited state<sup>49,50</sup> because the potential energy curve presents a very low energetic barrier to rotation around the vinyl-phenyl bonds, resulting in an almost flat surface, at least at ambient temperature, for torsion angles ranging between  $-30^\circ$  and  $+30^\circ$ , thus making trans-cis isomerization feasible.<sup>49</sup>

We have measured the emission spectra of the isolated molecule in acetonitrile solution finding an overall agreement with the data reported in the literature in the same solvent,<sup>34,51</sup> and in chloroform or in a polystyrene matrix.<sup>38</sup> The spectral deconvolution, presented in [Fig. 5](#), shows five main peaks at 334.5, 348.6, 365.3, 383.8, and 402.4 nm. The separation among these peaks is extremely regular ranging between  $1200$  and  $1300 \text{ cm}^{-1}$ , therefore, suggesting its vibronic origin. There are three  $A_g$  modes between  $1194$  and  $1322 \text{ cm}^{-1}$  (frequency values measured in benzene solution<sup>52</sup>) being by far the most intense, the one lying at a lower frequency and assigned to the =C-Ph stretching mode,<sup>53</sup> which can be, therefore, the mode responsible for the vibronic progression. The high frequency peak, about 3.7 eV, can be assigned as the 0-0 transition, nicely agreeing with the one-photon absorption spectrum.<sup>28</sup> This peak is considerably weaker than the two vibronic bands at 348.6 and 365.3, thus indicating a displacement of the relative minima in the  $S_0 \rightarrow S_1$  transition ascribable to the lengthening of the ethylenic group. On the contrary, the  $1^1B_u \rightarrow 1^1A_g$  emission spectra computed by Gagliardi *et al.*<sup>48</sup> present the 0-0 emission line as the strongest one. The reason for that should be searched in the geometry they adopted, with an ethylenic bond length of  $1.383 \text{ \AA}$ , therefore very close to the ambient pressure value of  $1.326 \text{ \AA}$  measured in the crystal by x-ray diffraction.<sup>30</sup>

The strong intensification of the high energy emission band above 8 GPa could be, therefore, related to the structural phase transition, which leads to a consistent contraction of the cell volume mainly due to a reduction of the  $b$  axis.<sup>16</sup> Since the  $b$  axis coincides with the direction along which the nanothreads form, also becoming the nanothread axis itself, this rearrangement of the molecules has been thought to favor the formation of stacks of slipped, nearly parallel molecules along this axis. This packing, and the continuous reduction of the  $b$  lattice parameter with

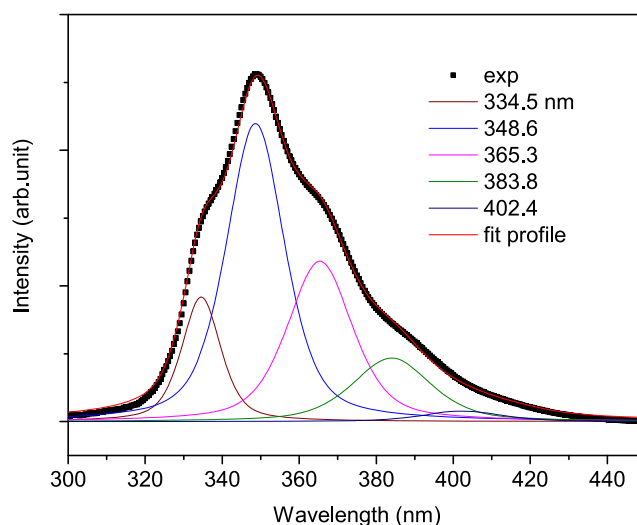


**FIG. 5.** Deconvolution of the one-photon ( $\lambda_{exc} = 290 \text{ nm}$ ) emission spectrum of stilbene in acetonitrile measured at ambient conditions. The peak maxima of the five bands used for reproducing the experimental pattern (symbols) are reported in the inset.

further pressure increase, could lead to a stabilization of the planar structure also in the lowest excited state with a delocalization of the excitation outside of the ethylenic group, making the equilibrium configuration of this state more and more similar to the fundamental one as the pressure is raised above 8 GPa. This conclusion contrasts with that recently reported by Gu *et al.*,<sup>43</sup> which overlooked the phase transition occurring around 8 GPa, which implies consistent structural changes,<sup>16</sup> and proposed, on the basis of DFT calculation, a progressive departure of the molecules from planarity consisting in a continuous increase of the torsion angle with pressure.

## V. CONCLUSIONS

Two-photon induced fluorescence is an important tool to monitor the electronic changes taking place in a molecular crystal at high pressure. The density increase produced by compression leads to an increasing overlap of molecular orbitals of adjacent molecules, causing electronic delocalization. This generally corresponds to a reduction of the energy gap between the ground and excited electronic states, especially in molecules containing conjugated  $\pi$  bonds. In fact,  $\pi$  orbitals are more sensitive to a density increase than  $\sigma$  orbitals because, under ambient conditions, they are more diffuse and characterized by a smaller overlap. For this reason, the  $\pi$ - $\pi^*$  transitions, among the lowest in energy, are strongly affected by compression. These changes can be extremely important to understand the mechanisms of the pressure induced reactivity in molecular systems.<sup>26,54,55</sup> Here, this technique has been applied to the study of crystalline stilbene to get insight into the mechanisms leading to the formation of double core carbon nanothread occurring above 16 GPa. This transformation is anticipated by a phase transition occurring around 7–9 GPa to a structure where the molecules presumably gain the correct orientation toward the nanothread formation.<sup>16</sup> Our results show, analogously to ambient pressure low temperature data, a freezing of the spectral diffusion below 1 GPa as deduced by the strong intensification and the blue shift of the higher energy band. The access to lower energy defect levels, corresponding to clusters of molecules having small conformational differences, is prevented by an increased energy barrier to be overcome for passing from one configuration to the other because of the larger stiffness of the local environment. Around 8 GPa, a phase transition, already observed by x-ray diffraction experiments,<sup>16</sup> is revealed by a slope change of the emission pattern and by the appearance and rapid intensification with pressure of the 0-0 emission line. The latter becomes the strongest peak above 15 GPa, suggesting a very similar geometry of the molecule in the fundamental and in the excited states, and thus a delocalization of the excitation from the ethylenic bond to the phenyl groups, which causes their progressive instability leading to the nanothread formation. The knowledge of the conformational changes occurring in the first electronic excited state suggests that the nanothread formation can be possibly induced at lower pressure by preparing through selective irradiation a certain amount of excited molecules that, although maintaining the molecular planarity, present an altered charge distribution on the phenyl ring that can trigger the reaction with neighboring ground state molecules.

## SUPPLEMENTARY MATERIAL

In the [supplementary material](#), we report the details of the fit procedure adopted to interpret the emission spectra and the XRD measurements performed to determine the stilbene crystal volume below 1 GPa.

## ACKNOWLEDGMENTS

We thank the European Laboratory for Nonlinear Spectroscopy (LENS) for hosting the research and the Deep Carbon Observatory and the “Fondazione CR Firenze” for their strong support. This research was supported by the following grants: Extreme Physics and Chemistry of Carbon: Forms, Transformations, and Movements in Planetary Interiors funded by the Alfred P. Sloan Foundation and Fondazione Cassa di Risparmio di Firenze under the project “Utilizzo dell’anisotropia strutturale nella sintesi di nanofili di carbonio diamond-like ad alta pressione.”

## AUTHOR DECLARATIONS

### Conflict of Interest

The authors have no conflicts to disclose.

### Author Contributions

**M. Agati:** Data curation (equal); Investigation (equal); Writing – review & editing (equal). **S. Fanetti:** Conceptualization (equal); Data curation (equal); Investigation (equal); Methodology (equal); Writing – review & editing (equal). **R. Bini:** Conceptualization (equal); Data curation (equal); Funding acquisition (equal); Writing – original draft (equal); Writing – review & editing (equal).

## DATA AVAILABILITY

The data that support the findings of this study are available within the article and its [supplementary material](#) and from the corresponding author upon reasonable request.

## REFERENCES

- <sup>1</sup>R. E. Roman, K. Kwan, and S. W. Cranford, *Nano Lett.* **15**, 1585 (2015).
- <sup>2</sup>J. F. R. V. Silveira and A. R. Muniz, *Carbon* **113**, 260 (2017).
- <sup>3</sup>D. Stojkovic, P. Zhang, and V. H. Crespi, *Phys. Rev. Lett.* **87**, 125502 (2001).
- <sup>4</sup>X.-D. Wen, R. Hoffmann, and N. W. Ashcroft, *J. Am. Chem. Soc.* **133**, 9023 (2011).
- <sup>5</sup>S. R. Barua, H. Quanz, M. Olbrich, P. R. Schreiner, D. Trauner, and W. D. Allen, *Chem. - Eur. J.* **20**, 1638 (2014).
- <sup>6</sup>T. C. Fitzgibbons, M. Guthrie, E.-s. Xu, V. H. Crespi, S. K. Davidowski, G. D. Cody, N. Alem, and J. V. Badding, *Nat. Mater.* **14**, 43 (2015).
- <sup>7</sup>X. Li, T. Wang, P. Duan, M. Baldini, H.-T. Huang, B. Chen, S. J. Juhl, D. Koeplinger, V. H. Crespi, K. Schmidt-Rohr *et al.*, *J. Am. Chem. Soc.* **140**, 4969 (2018).
- <sup>8</sup>S. Fanetti, M. Santoro, F. Alabarse, E. Berretti, and R. Bini, *Nanoscale* **12**, 5233 (2020).
- <sup>9</sup>M. M. Nobrega, E. Teixeira-Neto, A. B. Cairns, M. L. A. Temperini, and R. Bini, *Chem. Sci.* **9**, 254 (2018).
- <sup>10</sup>A. Biswas, M. D. Ward, T. Wang, L. Zhu, H.-T. Huang, J. V. Badding, V. H. Crespi, and T. A. Strobel, *J. Chem. Lett.* **10**, 7164 (2019).



- <sup>11</sup>S. Huss, S. Wu, B. Chen, T. Wang, M. C. Gerthoffer, D. J. Ryan, S. E. Smith, V. H. Crespi, J. V. Badding, and E. Elacqua, *ACS Nano* **15**, 4134 (2021).
- <sup>12</sup>M. D. Ward, W. S. Tang, L. Zhu, D. Popov, G. D. Cody, and T. A. Strobel, *Macromolecules* **52**, 7557 (2019).
- <sup>13</sup>A. Friedrich, I. E. Collings, K. F. Dziubek, S. Fanetti, K. Radacki, J. Ruiz-Fuertes, J. Pellicer-Porres, M. Hanfland, D. Sieh, R. Bini, S. J. Clark, and T. B. Marder, *J. Am. Chem. Soc.* **142**, 18907 (2020).
- <sup>14</sup>S. G. Dunning, L. Zhu, B. Chen, S. Chariton, V. B. Prakapenka, M. Somayazulu, and T. A. Strobel, *J. Am. Chem. Soc.* **144**, 2073 (2022).
- <sup>15</sup>D. Gao, X. Tang, J. Xu, X. Yang, P. Zhang, G. Che, Y. Wang, Y. Chen, X. Gao, X. Dong, H. Zheng, K. Li, and H.-k. Mao, *Proc. Natl. Acad. Sci. U. S. A.* **119**, e2201165119 (2022).
- <sup>16</sup>S. Romi, S. Fanetti, F. Alabarse, A. M. Mio, J. Haines, and R. Bini, *Nanoscale* **14**, 4614 (2022).
- <sup>17</sup>S. Romi, S. Fanetti, F. Alabarse, A. M. Mio, and R. Bini, *Chem. Sci.* **12**, 7048 (2021).
- <sup>18</sup>S. Romi, S. Fanetti, F. Alabarse, and R. Bini, *J. Phys. Chem. C* **125**, 17174 (2021).
- <sup>19</sup>S. Romi, S. Fanetti, F. G. Alabarse, R. Bini, and M. Santoro, *Chem. Mater.* **34**, 2422 (2022).
- <sup>20</sup>J. H. Williams, *Acc. Chem. Res.* **26**, 593 (1993).
- <sup>21</sup>P. Coppens, *Science* **158**, 1577 (1967).
- <sup>22</sup>X. Li, M. Baldini, T. Wang, B. Chen, E.-s. Xu, B. Vermilyea, V. H. Crespi, R. Hoffmann, J. J. Molaison, C. A. Tulk, M. Guthrie, S. Sinogeikin, and J. V. Badding, *J. Am. Chem. Soc.* **139**, 16343 (2017).
- <sup>23</sup>L. Ciabini, M. Santoro, F. A. Gorelli, R. Bini, V. Schettino, and S. Raugel, *Nat. Mater.* **6**, 39 (2007).
- <sup>24</sup>W. S. Tang and T. A. Strobel, *J. Phys. Chem. C* **124**, 25062 (2020).
- <sup>25</sup>M. Citroni, S. Fanetti, C. Bazzicalupi, K. Dziubek, M. Pagliai, M. M. Nobrega, M. Mezouar, and R. Bini, *J. Phys. Chem. C* **119**, 28560 (2015).
- <sup>26</sup>M. Citroni, R. Bini, P. Foggi, and V. Schettino, *Proc. Natl. Acad. Sci. U. S. A.* **105**, 7658 (2008).
- <sup>27</sup>V. Molina, M. Merchán, and B. O. Roos, *J. Phys. Chem. A* **101**, 3478 (1997).
- <sup>28</sup>M. de Wergifosse, A. L. Houk, A. I. Krylov, and C. G. Elles, *J. Chem. Phys.* **146**, 144305 (2017).
- <sup>29</sup>J. Harada and K. Ogawa, *J. Am. Chem. Soc.* **126**, 3539 (2004).
- <sup>30</sup>J. A. Bouwstra, A. Schouten, J. Kroon, and R. B. Helmholtz, *J. Acta Crystallogr., Sect. C: Cryst. Struct. Commun.* **40**, 428 (1984).
- <sup>31</sup>D. H. Waldeck, *Chem. Rev.* **91**, 415 (1991).
- <sup>32</sup>H. Görner and H. J. Kuhn, "Cis-trans photoisomerization of stilbenes and stilbene-like molecules," in *Advances in Photochemistry* (Wiley, 1994), Vol. 19.
- <sup>33</sup>S. Takeuchi, S. Ruhman, T. Tsuneda, M. Chiba, T. Taketsugu, and T. Tahara, *Science* **322**, 1073 (2008).
- <sup>34</sup>A. Weigel and N. P. Ernsting, *J. Phys. Chem. B* **114**, 7879 (2010).
- <sup>35</sup>S. V. Budakovskiy, N. Z. Galunov, A. Y. Rybalkooleg, A. Tarasenko, and V. V. Yarychkin, *Mol. Cryst. Liq. Cryst.* **385**, 71 (2002).
- <sup>36</sup>K. Zhao, L. Chen, H. P. Guo, J. L. Ruan, S. Y. He, Z. B. Zhang, and X. P. Ouyang, *J. Instrum.* **13**, P10001 (2018).
- <sup>37</sup>N. Ostapenko, M. Ilchenko, Y. Ostapenko, O. Kerita, V. Melnik, E. Klishevich, N. Galunov, I. Lazarev, and M. Chursanova, *Mol. Cryst. Liq. Cryst.* **671**, 104 (2018).
- <sup>38</sup>R. Karpicz, N. Ostapenko, Y. Ostapenko, Y. Polupan, I. Lazarev, N. Galunov, M. Macernis, D. Abramavicius, and L. Valkunas, *Phys. Chem. Chem. Phys.* **23**, 3447 (2021).
- <sup>39</sup>S. Fanetti, M. Citroni, and R. Bini, *J. Phys. Chem. B* **115**, 12051 (2011).
- <sup>40</sup>H. K. Mao, P. M. Bell, J. W. Shaner, and D. J. Steinberg, *J. Appl. Phys.* **49**, 3276 (1978).
- <sup>41</sup>R. Bini, R. Ballerini, G. Pratesi, and H. J. Jodl, *Rev. Sci. Instrum.* **68**, 3154 (1997).
- <sup>42</sup>R. M. Hochstrasser, *J. Mol. Spectrosc.* **8**, 485 (1962).
- <sup>43</sup>Y. Gu, G. Shao, Z. Tian, H. Li, K. Wang, and B. Zou, *Chin. Phys. B* **31**, 017901 (2022).
- <sup>44</sup>H. Bässler, *Phys. Status Solidi B* **175**, 15 (1993).
- <sup>45</sup>S. T. Hoffmann, H. Bässler, J.-M. Koenen, M. Forster, U. Scherf, E. Scheler, P. Strohriegel, and A. Köhler, *Phys. Rev. B* **81**, 115103 (2010).
- <sup>46</sup>A. Hoekstra, P. Meertens, and A. Vos, *Acta Crystallogr., Sect. B: Struct. Sci., Cryst. Eng. Mater.* **31**, 2813 (1975).
- <sup>47</sup>H. Takeshita, Y. Suzuki, Y. Hirai, Y. Nibu, H. Shimada, and R. Shimada, *Bull. Chem. Soc. Jpn.* **77**, 477 (2004).
- <sup>48</sup>L. Gagliardi, G. Orlandi, V. Molina, P.-Å. Malmqvist, and B. Roos, *J. Phys. Chem. A* **106**, 7355 (2002).
- <sup>49</sup>O. Lhost and J. L. Brédas, *J. Chem. Phys.* **96**, 5279 (1992).
- <sup>50</sup>G. Hohlneicher, R. Wrzal, D. Lenoir, and R. Frank, *J. Phys. Chem. A* **103**, 8969 (1999).
- <sup>51</sup>V. Vicinelli, P. Ceroni, M. Maestri, M. Lazzari, V. Balzani, S.-K. Lee, J. van Heyst, and F. Vögtle, *Org. Biomol. Chem.* **2**, 2207 (2004).
- <sup>52</sup>A. Bree and M. Edelson, *Chem. Phys.* **51**, 77 (1980).
- <sup>53</sup>Z. Meic and H. Güsten, *Spectrochim. Acta* **34A**, 101 (1978).
- <sup>54</sup>S. Fanetti, M. Ceppatelli, M. Citroni, and R. Bini, *J. Phys. Chem. C* **116**, 2108 (2012).
- <sup>55</sup>S. Fanetti, M. Citroni, and R. Bini, *J. Phys. Chem. C* **118**, 13764 (2014).